☙

Charge neutrality and band-gap tuning of epitaxial graphene on SiC by molecular doping

C. Coletti,[1,*] C. Riedl,[1] D. S. Lee,[1] B. Krauss,[1] L. Patthey,[2] K. von Klitzing,[1] J. H. Smet,[1] and U. Starke[1,†]

[1]*Max-Planck-Institut für Festkörperforschung, Heisenbergstr. 1, D-70569 Stuttgart, Germany*
[2]*Paul Scherrer Institut, CH-5232 Villigen PSI, Switzerland*

Epitaxial graphene on SiC(0001) suffers from strong intrinsic n-type doping. We demonstrate that the excess negative charge can be fully compensated by noncovalently functionalizing graphene with the strong electron-acceptor tetrafluorotetracyanoquinodimethane (F4-TCNQ). Charge neutrality can be reached in monolayer graphene as shown in electron-dispersion spectra from angular-resolved photoemission spectroscopy. In bilayer graphene the band-gap that originates from the SiC/graphene interface dipole increases with increasing F4-TCNQ deposition and, as a consequence of the molecular doping, the Fermi level is shifted into the band-gap. The reduction in the charge-carrier density upon molecular deposition is quantified using electronic Fermi surfaces and Raman spectroscopy. The structural and electronic characteristics of the graphene/F4-TCNQ charge-transfer complex are investigated by x-ray photoelectron spectroscopy and ultraviolet photoelectron spectroscopy. The doping effect on graphene is preserved in air and is temperature resistant up to 200 °C. Furthermore, graphene noncovalent functionalization with F4-TCNQ can be implemented not only via evaporation in ultrahigh vacuum but also by wet chemistry.

I. INTRODUCTION

The electronic properties of graphene, such as large room-temperature mobilities, comparable conductivities for electrons and holes and the ability for charge-carrier operation via the field effect, make it an excellent candidate for carbon-based nanoelectronics.[1–3] However, the limited size of graphene flakes from conventional micromechanical cleaving[1] requires individual selection and handling which makes device fabrication cumbersome. In contrast, epitaxial graphene grown on silicon carbide (SiC) offers realistic prospects for large scale graphene samples.[4–6] Unfortunately, as-grown epitaxial graphene is electron doped as a result of the graphene/SiC interface properties.[7–11] This doping translates into a displacement of the Fermi energy, E_F, away from the Dirac point energy E_D where the π bands cross so that the ambipolar properties of graphene cannot be exploited. Several approaches can be used to remove or compensate this excess charge. One that has recently been introduced is the structural decoupling of the graphene layers from the substrate using hydrogen intercalation.[12] Also, chemical gating techniques are very promising to tune the carrier concentration as demonstrated recently in low-temperature experiments on graphene flakes.[13,14] Analogously, a possibility to compensate the n doping in epitaxial graphene is to extract the surplus negative carriers, i.e., in the language of semiconductors, to accomplish a method of hole injection.

Similar to the case of carbon nanotubes,[15,16] injection of holes in graphene can be achieved via surface adsorption of gas molecules such as O_2 or the paramagnetic NO_2.[17,18] In contrast, NH_3 and alkali metals such as potassium are known to act as electron donors in carbon based materials.[7,15,18,19] However, the high reactivity of NO_2, NH_3, and of alkali atoms makes those materials ill-suited as practical dopants. This is illustrated by the need of cryogenic temperatures and ultra high vacuum conditions to stably adsorb NO_2 and potassium on graphene surfaces.[7,17] An approach that promises to control the carrier type and concentration in graphene in a simple and reliable way is that of surface-transfer doping via organic molecules.[20] A variety of aromatic and nonaromatic molecules and even organic free radicals can be used to control graphene doping.[21–25] Many of these molecules possess good thermal stability, have limited volatility after adsorption and can be easily applied via wet chemistry. An effective p-type dopant is the strong electron acceptor tetrafluorotetracyanoquinodimethane (F4-TCNQ). It has a very high electron affinity (i.e., $E_{ea}=5.24$ eV) and has been used successfully as a state of the art p-type dopant in organic light-emitting diodes,[20,26–28] carbon nanotubes,[29–31] and on other materials.[32,33] Recently, the existence of a p-doping effect of F4-TCNQ on graphene has been suggested theoretically[34] and experimentally.[25]

In the present paper we give direct evidence that the excess negative charge in epitaxial monolayer graphene can be fully compensated by functionalizing its surface with F4-TCNQ. Electron-dispersion spectra and Fermi-surface maps measured via angle-resolved photoemission spectroscopy (ARPES) qualitatively and quantitatively evaluate the reduction in charge-carrier density and show that charge neutral graphene can be ultimately obtained. X-ray photoelectron spectroscopy (XPS) and ultraviolet photoelectron spectroscopy (UPS) elucidate the structural and electronic characteristics of the graphene/F4-TCNQ charge-transfer complex. Raman spectroscopy of the G phonon peak corroborates the doping reversal and shows that the carrier concentration can be trimmed by laser induced desorption of molecules. Moreover, we investigate the effects of F4-TCNQ on the band structure of bilayer graphene. By presenting a band-gap,[7–10] bilayer graphene is particularly attractive for the implementation of electronic devices such as field-effect transistors provided that the intrinsic doping can be compensated. Here we demonstrate that F4-TCNQ not only renders bilayer graphene semiconducting thanks to the full compensation of the excess negative-charged carriers but also increases the
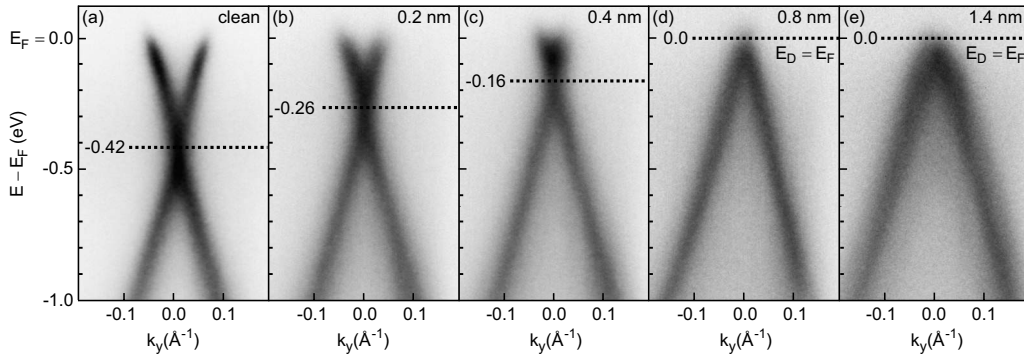
FIG. 1. Dispersion of the π bands measured with UV-excited ARPES around the $\bar{K}$ point of the graphene Brillouin zone for (a) an as-grown graphene monolayer on SiC(0001) and [(b)–(e)] for the same sample covered with an increasing amount of F4-TCNQ molecules. The momentum scans are taken perpendicular to the $\bar{\Gamma}\bar{K}$ direction in reciprocal space. The Fermi level E_F shifts progressively toward the Dirac point (E_D, dotted black line) with increasing nominal thickness of the deposited F4-TCNQ film. (d) Charge neutrality ($E_F=E_D$) is reached for a molecular coverage of 0.8 nm. (e) When depositing additional molecules the Fermi level does not shift any further.

band-gap size to more than double of its initial value. We show that the molecular layer is stable when exposed to air. The doping effect is preserved up to 200 °C and is totally reversible by annealing the sample at higher temperatures. The molecular coverage can be precisely controlled when using a molecular evaporator but the dopants can also be applied by wet chemistry, i.e., in a technologically convenient way.

II. EXPERIMENTAL

Epitaxial graphene was grown in UHV by thermal Si sublimation[5] on hydrogen etched,[35,36] atomically flat 6H-SiC(0001) crystals. The samples were characterized with low-energy electron diffraction and ARPES. Subsequently, F4-TCNQ molecules (7,7,8,8-Tetracyano-2,3,5,6-tetrafluoroquinodimethane, Sigma Aldrich, 97% purity) were deposited on the graphene/SiC substrates by thermal evaporation from a resistively heated crucible. For comparison also the nonfluorinated version of F4-TCNQ, i.e., tetracyanoquinodimethane (TCNQ) was deposited (7,7,8,8-tetracyanoquinodimethane, Sigma Aldrich, 98% purity). In house ARPES measurements were carried out at room temperature using monochromatic He II radiation ($h\nu$ =40.8 eV) from a UV discharge source with a display analyzer oriented for momentum scans perpendicular to the $\bar{\Gamma}\bar{K}$ direction of the graphene Brillouin zone. The Fermi-surface data were extracted from ARPES experiments using synchrotron radiation from the Swiss Light Source of the Paul Scherrer Institut, Switzerland, at the Surface and Interface Spectroscopy beamline. The end station allows, using a display analyzer and a sample manipulator with three rotational degrees of freedom, for fast high-resolution two-dimensional electronic-dispersion measurements. XPS measurements were performed using photons from a nonmonochromatic Mg $K\alpha$ source ($h\nu$=1253.6 eV). The stability of the molecular layers under UV and x-ray irradiation was verified by exposing 3 h and well over 13 h, respectively. The thickness of the deposited molecular layers was estimated from XPS spectra calibrated through a comparison to spectra for a well-

characterized surface phase of TCNQ on Cu(100) measured under identical conditions.[37] Different deposition rates ranging from 0.07 to 0.5 Å/min and sample temperatures between −140 and 25 °C were tested for the sample preparation. No influence on the doping results was found when the same amount of molecules was deposited. Work-function measurements and the analysis of molecular orbitals were performed via normal emission UPS using monochromatic He I radiation ($h\nu$=21.21 eV) from our UV source. During the work-function measurements a bias of −30 V was applied to the sample in order to distinguish between the analyzer and the sample cutoff and to more efficiently collect the inelastically scattered low kinetic-energy electrons into the analyzer. Raman spectra were measured under ambient conditions using an Argon ion laser with a wavelength of 488 nm at a power level of 12 mW and a laser spot size of ≈ 1 μm in diameter. In order to apply the molecular layer on graphene via wet chemistry F4-TCNQ was dissolved in either chloroform or dimethyl sulfoxide (DMSO) until saturation. Before ARPES characterization the sample was left immersed in the solution for 12 h.

III. F4-TCNQ ON MONOLAYER GRAPHENE

The doping level of the graphene layers can be precisely monitored with ARPES measurements of the π-band dispersion around the $\bar{K}$ point of the graphene Brillouin zone as previously established.[7–11] As shown in Fig. 1(a) for an as-grown monolayer of graphene on SiC(0001) the Fermi level E_F is located about 0.42 eV above the Dirac point E_D. This corresponds to the well-established charge-carrier-concentration value of $n \approx 1 \times 10^{13}$ cm^{-2} for as grown graphene. For increasing amounts of deposited F4-TCNQ E_F moves back toward E_D as illustrated in Figs. 1(b)–1(d). Meanwhile the bands remain sharp, which indicates that the integrity of the graphene layer is preserved. Evidently, deposition of F4-TCNQ activates electron transfer from graphene toward the molecule thus neutralizing the excess doping induced by the substrate. As the figure shows the electron concentration in the graphene layer can be tuned precisely by
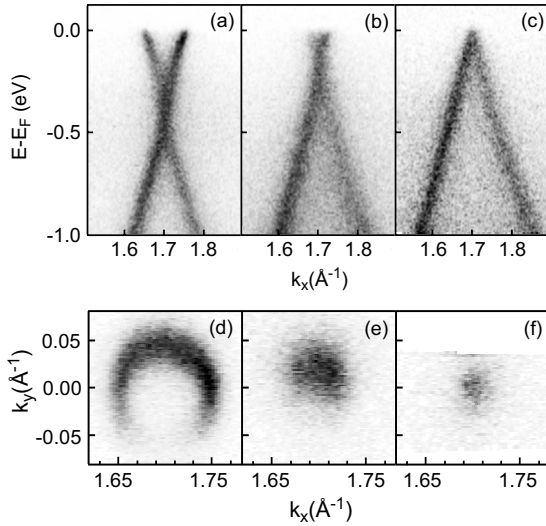
FIG. 2. Dispersion of the π band around the $\bar{K}$ point of the graphene Brillouin zone measured by ARPES with synchrotron light in scans oriented parallel to the $\bar{\Gamma}\bar{K}$ direction for (a) a pristine epitaxial graphene monolayer, (b) an intermediate F4-TCNQ coverage, and (c) the F4-TCNQ coverage leading to charge neutrality. Panels (d)–(f) show the corresponding constant energy maps at E_F. From these Fermi-surface maps we extract a charge carrier concentration of $7.3 \pm 0.2 \times 10^{12}$ cm^{-2} for the pristine graphene, $9 \pm 2 \times 10^{11}$ cm^{-2} for the intermediate coverage, and $1.5 \pm 2 \times 10^{11}$ cm^{-2} for full coverage. All the spectra shown were acquired with circular polarized light with a photon energy of 30 eV and at a sample temperature of 80 K.

varying the amount of deposited molecules. When we deposit a 0.8-nm-thick layer of molecules, charge neutrality is reached, i.e., $E_F = E_D$. For a nominal thickness of the molecular film above 0.8 nm no additional shift of the Fermi energy is observed as seen in Fig. 1(e), which indicates that the charge transfer saturates.

For a detailed quantitative determination of the carrier concentrations, high-resolution ARPES data acquired using synchrotron radiation were analyzed. Figure 2 compares the π-band dispersion [(a)–(c)] and constant energy maps [(d)–(f)] at E_F for a clean graphene monolayer [(a) and (d)], an intermediate F4-TCNQ coverage [(b) and (e)], and charge-transfer saturation at full coverage [(c) and (f)]. The charge-carrier concentration can be derived precisely from the size of the Fermi-surface pockets as $n = (k_F - k_{\bar{K}})^2 / \pi$, where $k_{\bar{K}}$ denotes the wave vector at the boundary of the graphene Brillouin zone. The Fermi-surface pocket radius is extracted by using Lorentzian fits of the maxima of the momentum-distribution curves of the electronic-dispersion spectra in panels [(a)–(c)]. The corresponding carrier concentrations are 7.3×10^{12} cm^{-2}, 9×10^{11} cm^{-2}, and 1.5×10^{11} cm^{-2} for the clean graphene monolayer, the intermediate and the higher coverage, respectively. The error bar for the reported carrier concentrations is $\pm 2 \times 10^{11}$ cm^{-2} and was determined from the variance of the Lorentzian fits.

IV. CHARACTERIZATION OF THE CHARGE-TRANSFER COMPLEX

The location of the charge-transfer process within the F4-TCNQ molecule can be elucidated by core-level analysis using XPS. N 1s and F 1s core-level-emission spectra for different amounts of deposited F4-TCNQ are displayed in Fig. 3. For the N 1s spectra of panel (a) a line-shape analysis reveals two main components centered at binding energies (BE) of 398.3 and 399.6 eV. This indicates that different N species exist in the deposited molecular film. In agreement with the literature[25,38] the peak at 398.3 eV is assigned to the anionic species N^{-1} while the 399.6 eV component is attributed to the neutral N^0 species. The additional broad component at 401.7 eV likely originates from shake-up processes in view of its energy location and the relative intensity (approximately 20%) as compared to the main peak.[39] The F 1s
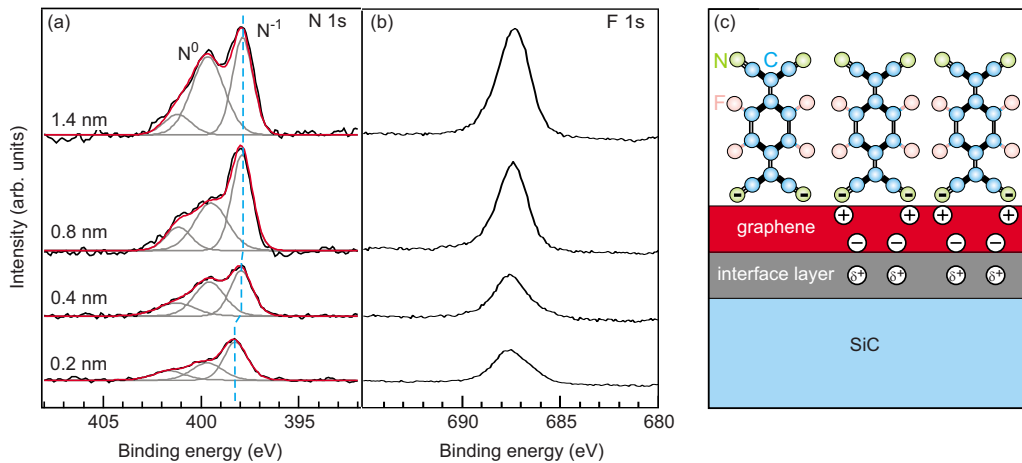

FIG. 3. (Color online) [(a) and (b)] XPS spectra of the (a) N 1s and (b) F 1s core-level emission regions from submonolayer (bottom spectrum) to multilayer (top spectrum) amounts of F4-TCNQ deposited on a monolayer of graphene which has been grown epitaxially on SiC(0001). Three different components are fitted into the N 1s region and are assigned to N^{-1} and N^0 species and to a shake-up process. The blue dashed line indicates the exact energy position of the N^{-1} component as it shifts with molecular layer thickness. (c) Schematic of a F4-TCNQ layer deposited on top of a graphene layer grown on SiC. The charges induced in the graphene layer due to the interface dipole and the molecular charge transfers are indicated.
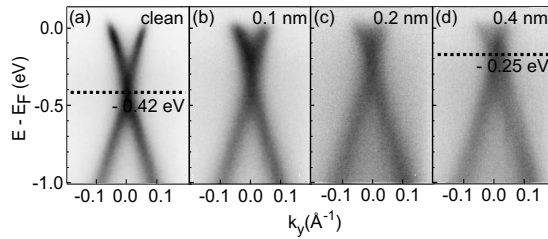
FIG. 4. Dispersion of the π bands measured with ARPES through the $\bar{K}$ point of the graphene Brillouin zone for (a) a pristine graphene monolayer grown on SiC(0001) and [(b)–(d)] for increasing amounts of TCNQ deposited on graphene. The Fermi level (E_F) shifts progressively toward the Dirac point (E_D, black dotted line) for increasing molecular coverage up to a value of $E_D - E_F = -0.25$ eV.

spectra in Fig. 3(b) are in contrast dominated by a single component. Only at low coverages a weak asymmetry develops. The appearance of the N^{-1} anion species indicates that the electron transfer takes place through the C≡N groups of the molecules while the fluorine atoms are largely inactive. A similar mechanism with electronically active cyano groups has been found for F4-TCNQ on other surfaces.[39–41] However, in the present case not all C≡N groups are involved in the charge transfer process. While for low molecular coverages the N^{-1} species dominate (71%), for coverages from 0.4 to 0.8 nm about 45% of the C≡N groups are uncharged (N^0) as determined from the peak areas (zeroth momentum) of the fitted components. This indicates that when the films are densely packed, most of the molecules are standing upright as sketched in Fig. 3(c) (apparently, in dilute layers not all molecules are arranged perpendicular to the surface). We note that this result is only valid for the initial molecular layer and is different than what was recently proposed for multilayers (5 nm) of F4-TCNQ.[20] The energy position of the different core-level peaks shifts with increasing molecular coverage as indicated by the blue dashed line in Fig. 3(a). For 0.8 nm nominal film thickness this shift is exactly the same as the shift of the π bands with respect to the Fermi energy E_F (i.e., 0.4 eV for saturation) in agreement with our working hypothesis of a strong electronic coupling between the F4-TCNQ molecule and the graphene surface. At coverages larger than 0.8 nm, the shift of both the N^{-1} peak and the band structure saturates. Only the N^0 peak continues to grow indicating the formation of a charge neutral second layer of molecules. The saturation effect at 0.8-nm nominal film thickness also supports the model of a dense layer of upright standing molecules since the size of an F4-TCNQ molecule along its axis is indeed about 0.8 nm.

A comparison of the experimental band shifts when using the nonfluorinated version of the F4-TCNQ molecule, i.e., TCNQ, shows that the charge transfer is greatly enhanced when the F species are present, even though they are not directly involved in the charge-transfer process. With TCNQ, which has a much smaller electron affinity than F4-TCNQ (i.e., 2.8 eV for TCNQ compared to 5.24 eV for F4-TCNQ), the Fermi energy remains at least 0.25 eV above the Dirac point (see Fig. 4). The maximum shift of the band structure measured upon TCNQ deposition is obtained for a molecular
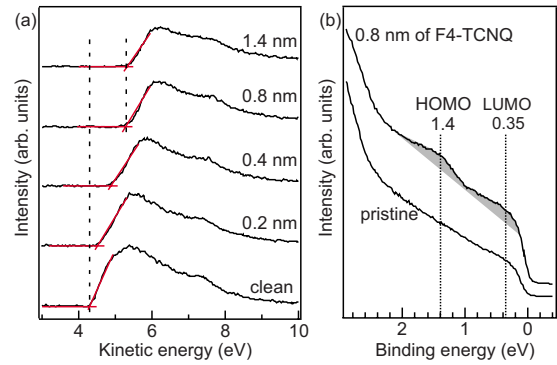

FIG. 5. (Color online) (a) Secondary electron cut-off region measured by normal emission UPS ($h\nu = 21.21$ eV) for increasing nominal thickness of a F4-TCNQ film deposited on epitaxial monolayer graphene on SiC(0001) in order to estimate the work-function change ($\Delta\Phi$). (b) Near E_F UPS spectra for clean graphene (bottom) and graphene with 0.8 nm of deposited F4-TCNQ (top). The shaded areas highlight the emerging features following F4-TCNQ deposition and are attributed to the HOMO (at 1.4 eV) and to the LUMO which has partially shifted below E_F (at 0.35 eV).

coverage of 0.4 nm [see Fig. 4(d)] and no additional shift is observed for higher amounts of deposited molecules.

Additional evidence for the formation of charge-transfer complexes in the case of F4-TCNQ is obtained from the work-function measurements shown in Fig. 5(a). The kinetic energies are plotted after correction for the applied bias and the analyzer work function so that the sample work function is directly obtained from the intersection between the base line of the spectrum and a linear fit to the tail of the sample secondary electron cutoff. The work function (Φ) gradually increases from 4.28 eV for as-grown epitaxial graphene to a maximum value of 5.29 eV for 0.8 nm of F4-TCNQ on top of graphene and saturates for larger molecular coverages. The measured shift ($\Delta\Phi \approx 1$ eV) contains both the band bending at the graphene surface (0.4 eV) and an additional contribution from the interface dipole generated by the charge transfer (i.e., ≈ 0.6 eV).

An analysis of the position of the highest occupied molecular orbitals (HOMO) and lowest unoccupied molecular orbitals (LUMO) of F4-TCNQ with respect to the Fermi level using normal emission UPS corroborates further that the molecule gets charged. The low BE portion of the UPS spectra of a graphene sample with a 0.8-nm molecular coverage exhibits two additional shoulders, which are not observed for pristine epitaxial graphene. They are located at 1.4 and 0.35 eV [see Fig. 5(b)]. In agreement with the literature,[25,33,42] the higher BE peak is attributed to the HOMO and the lowest BE peak to the (now partially populated) LUMO of the molecule. Even though the HOMO of the pristine molecule is typically found at higher BE values[43] and the LUMO is expected for negative BE values, filling of the former LUMO of F4-TCNQ with one electron generates a negative polaron.[42] Hence, the LUMO is stabilized, i.e., the binding energy of the newly occupied state is increased. In contrast, the former HOMO is destabilized (lower BE).
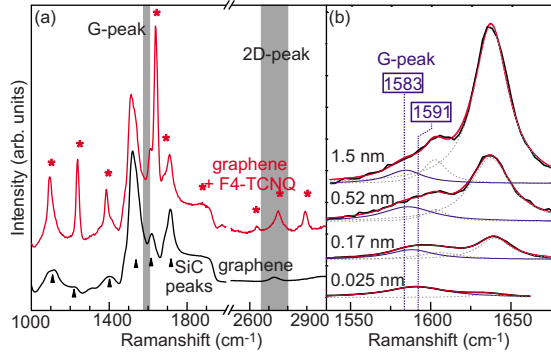
FIG. 6. (Color online) (a) Raman spectrum of pristine (bottom black trace) and F4-TCNQ-modified (top red trace) monolayer graphene epitaxially grown on SiC(0001). Molecular peaks are marked with stars and the peaks related to SiC with arrows. The G- and 2D-peak regions of graphene are shaded. (b) Differential Raman spectra for different coverages of the F4-TCNQ molecular film ranging from 1.5 to 0.025 nm (see main text). The gray dashed lines are Lorentzians to fit the molecular peaks. The blue solid line is the extracted graphene contribution to the Raman spectrum (G peak).

V. RAMAN SPECTROSCOPY ANALYSIS

The influence of the F4-TCNQ coverage on the vibrational and electronic properties of the graphene layer was also studied under ambient conditions with Raman spectroscopy. Figure 6(a) compares Raman spectra for an as-grown epitaxial monolayer of graphene (bottom trace) and for a sample that has been covered with a 1.5-nm-thick F4-TCNQ layer (top trace). Peaks related to the SiC substrate are marked by arrows. The two-dimensional (2D) peak of graphene is highlighted with gray shading. So is the G peak. The latter is barely visible due to overwhelming contributions of the SiC substrate in this wavelength range.[44] The Raman spectrum for graphene covered with F4-TCNQ reveals numerous additional features that are marked by stars. By illuminating a sample that is covered with F4-TCNQ molecules with the Argon laser light it is possible to gradually remove the deposited molecules through evaporation. Features associated with the SiC substrate and graphene hardly change while the peaks attributed to the F4-TCNQ molecules decrease in amplitude. Laser heating can therefore be used to trim the molecule coverage and hence tune the charge-carrier concentration in graphene. In a confocal arrangement it is therefore possible to spatially modulate the doping level. The charge-carrier concentration can be extracted from a detailed inspection of the G peak. In order to eliminate the large contributions of the SiC substrate, it is instrumental to analyze differential spectra obtained by subtracting the Raman data of the clean hydrogen-etched SiC substrate from the spectrum of the F4-TCNQ-modified graphene layer on top of SiC.[44,45] The evolution of the G peak upon successive laser illumination, i.e., for successively reduced amounts of F4-TCNQ, is illustrated in Fig. 6(b). Only the spectral region from 1530 to 1700 cm^{-1} centered around the G peak is shown. The spectra can be decomposed into three peaks. Two molecular peaks at ≈ 1602 and ≈ 1637 cm^{-1} decrease with the laser exposure. The molecu-

lar coverage before laser exposure was calibrated with XPS [top curve in panel (b)]. The other molecular coverages marked in Fig. 6(b) are calculated from the relative intensity of the molecular peaks. The intensity of the remaining peak, which we attribute to the G phonons of graphene, is approximately constant and not influenced by laser exposure. The peak position shifts however from ≈ 1583 to ≈ 1591 cm^{-1}. In graphene the carrier density enters the electron-phonon coupling and causes phonon stiffening when the carrier density increases. The G-peak position of the F4-TCNQ saturated sample (1583.3 ± 0.9 cm^{-1}) is nearly the same as for charge neutral graphene flakes.[46,47] This is consistent with the ARPES data. As the molecules are successively removed, the G-peak blueshifts and finally reaches 1591 cm^{-1}, the value for clean monolayer graphene on SiC exposed to air.[44] This G-peak position corresponds to a charge-carrier concentration of $\approx 5 \times 10^{12}$ cm^{-2} (Refs. 46 and 47) or a band-gap shift of $E_F - E_D \approx 0.3$ eV. We note, that this value is less than measured by ARPES ($E_F - E_D = 0.42$ eV) due to the additional doping when the sample is exposed to air as reported previously.[44]

VI. F4-TCNQ ON BILAYER GRAPHENE

For bilayers the band shift caused by the intrinsic n doping of epitaxial graphene on SiC is slightly lower than for epitaxial monolayers, namely, about 0.3 eV. In addition, the electric dipole present at the graphene/SiC interface imposes an electrostatic asymmetry between the layers which causes a band-gap to open by roughly 0.1 eV (Refs. 7–10) as seen from the ARPES data in Fig. 7(a). In the figure bands obtained from tight-binding calculations are superimposed to the dispersion plot. This facilitates an analytical evaluation of the Dirac energy position and the size of the band-gap. The calculations are based on a symmetric bilayer Hamiltonian as described by McCann and Fal'ko.[48] We note that, due to the inevitable inhomogeneity of UHV-prepared graphene samples and the beam spot size, the ARPES data contain contributions of film areas with different thickness. This can be seen by a comparison with data from a sample prepared at a slightly lower temperature in Fig. 7(f). Here, the contribution from monolayer patches is notably stronger and obstructs a clear view on the bilayer bands. The sketch in panel (g) identifies the band contributions stemming from different graphene thicknesses. In the sample used for panel (a) the bilayer bands are well isolated although trilayer contributions are clearly present. Similar to the monolayer case, F4-TCNQ deposition onto this sample causes a progressive shift of the bilayer bands, i.e., a reduction in the intrinsic n-type doping. This is illustrated in the measured and calculated dispersion plots in Figs. 7(b)–7(e). Concurrent with the drop of $E_F - E_D$, the size of the band-gap increases as seen from the bands fitted with the tight-binding simulations. The band fitting retrieves the energy at the bottom of the lowest conduction band E_{cond} and at the top of the uppermost valence band E_{val}. From these values the energy gap E_g and the midgap or Dirac energy E_D are derived. The corresponding energies are marked in panel (c). The evolution of the characteristic energies of these fitted bands with the amount of
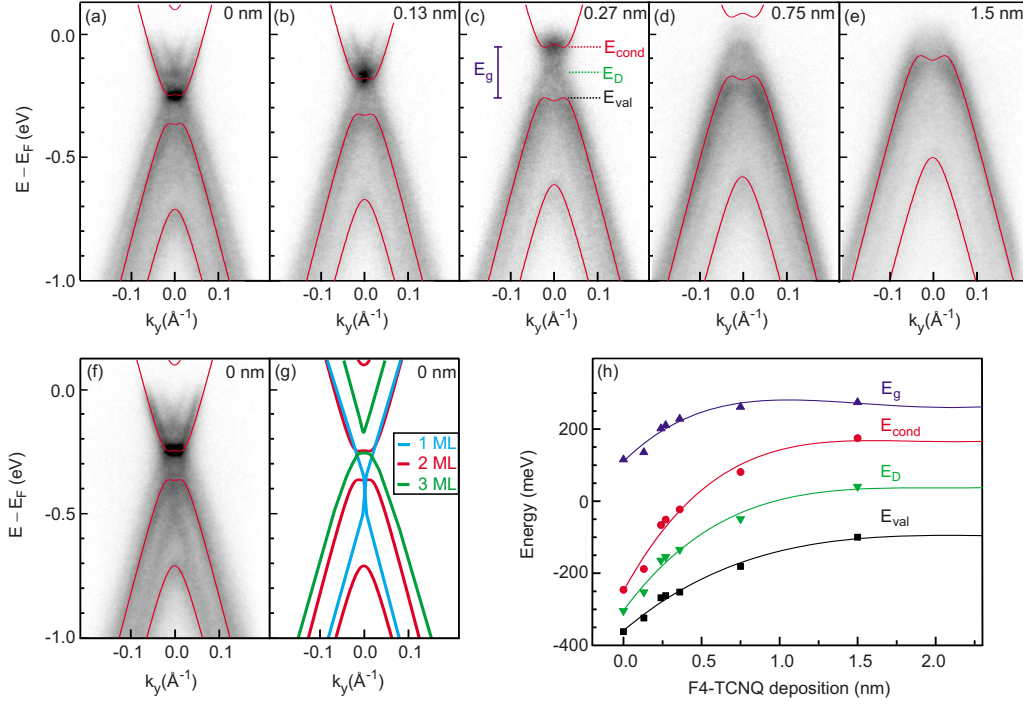
FIG. 7. (Color online) ARPES band-structure plots measured perpendicular to the $\overline{\Gamma}\overline{K}$ direction for an epitaxially grown graphene bilayer on SiC(0001) (a) without F4-TCNQ coverage and [(b)–(e)] with increasing amounts of F4-TCNQ. Bands calculated within a tight-binding model are superimposed to the experimental data. (f) ARPES data showing the band structure of an epitaxial graphene bilayer prepared at a lower annealing temperature. Contributions from monolayer domains are evident. (g) Schematic band structure of monolayer, bilayer, and trilayer epitaxial graphene. (h) Evolution of the energy gap E_g, the gap midpoint or Dirac point E_D, the minimum of the lowest conduction band E_{cond}, and the maximum of the uppermost valence band E_{val} as a function of molecular coverage. The evolution of the energies for higher molecular coverages (up to 5 nm, not shown) confirms charge-transfer saturation. The definition of the energies is included in panel (c).

deposited molecules is plotted in Fig. 7(h). The band-gap E_g increases from 116 meV for a clean as-grown bilayer to 275 meV when a 1.5-nm-thick layer of F4-TCNQ molecules has been deposited. We verified that no further charge transfer occurs for higher amounts of deposited molecules. The Fermi energy moves into the band-gap for a molecular layer thickness of 0.4 nm. Hence the bilayer is turned from a conducting system into a truly semiconducting layer. The increase in the band-gap indicates that the molecular deposition increases the on-site Coulomb potential difference between both layers. From the tight-binding calculations we get an increase in the on-site Coulomb interaction from 0.12 eV for a clean bilayer to 0.29 eV for a bilayer with a molecular coverage of 1.5 nm.[49] This increase can be attributed to an increased electrostatic field due to the additional dipole developing at the graphene/F4-TCNQ interface.

VII. THERMAL STABILITY AND CHEMICAL APPLICATION OF THE MOLECULES

An important aspect of the F4-TCNQ/graphene system is the robustness of its preparation: the Raman experiments after transport through ambient environment already demonstrated that the charge-transfer complex is stable in air. On a monolayer sample covered with a multilayer of F4-TCNQ molecules the band structure was measured with ARPES be-

fore and after several hours of air exposure. This experiment revealed no change in the band structure. XPS measurements also confirmed the inert nature of the graphene substrate. The experiment with laser-light exposure suggests that the F4-TCNQ layer is sensitive to temperature. The volatility of F4-TCNQ was probed in UHV by stepwise annealing a sample with a molecular coverage of 1.5 nm. The sample was annealed repeatedly for 1 min at successively higher temperatures between 25 °C and 230 °C in steps of about 25°. After each annealing step the shift of the Fermi level E_F with respect to the Dirac energy E_D was determined from ARPES spectra recorded at room temperature. As the annealing temperature increased the difference between the Dirac energy and the Fermi energy increased back to the value of a pristine graphene layer. This increase is considered direct evidence for molecular desorption from the graphene surface. As is evident from Fig. 8(a), desorption of the molecules is initiated at temperatures around 75 °C and completed at 230 °C. Since thermal desorption is amplified by UHV conditions we anticipate that even higher temperatures are needed under atmospheric pressure to remove the entire molecular layer. Finally, we demonstrate that the F4-TCNQ layer can also be applied by immersing the sample in a chemical F4-TCNQ solution. Two solvents were tested to apply the molecular layer on graphene via wet chemistry: chloroform and DMSO. ARPES spectra taken immediately after introduction into UHV show a considerable background
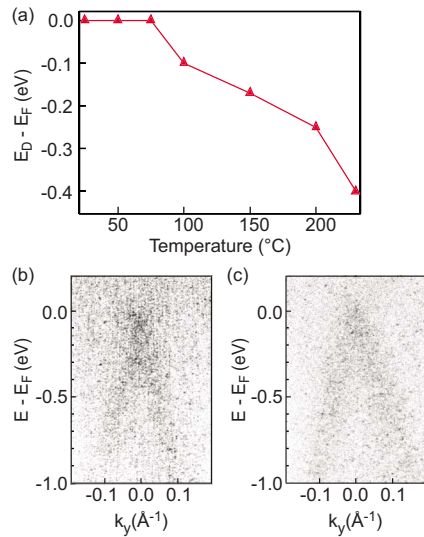
FIG. 8. (Color online) (a) Shift of the Fermi level E_F with respect to the Dirac energy E_D as a function of temperature during annealing of F4-TCNQ covered epitaxial monolayer graphene on SiC(0001). The shift was determined from ARPES data recorded after each annealing step in UHV of a graphene sample with an initial molecular coverage of 1.5 nm. (b) Incomplete shift of the π-band dispersion after F4-TCNQ wet chemical application in chloroform. (c) π-band dispersion after F4-TCNQ wet chemical application in DMSO. Charge neutrality is achieved, as indicated by $E_F = E_D$.

due to contamination by residual chemicals from the solution as displayed in Figs. 8(b) and 8(c). Nevertheless, the shift of the band structure is clearly visible and in the case of F4-

TCNQ wet chemical application in DMSO [panel (c)] charge neutrality (i.e., $E_F = E_D$) is achieved.

VIII. CONCLUSION

In conclusion, we have demonstrated that the band structure of epitaxial graphene on SiC(0001) can be precisely tailored by functionalizing the graphene surface with F4-TCNQ molecules. Charge neutrality can be achieved for monolayer and bilayer graphene. A charge-transfer complex is formed by the graphene film and the F4-TCNQ molecular overlayer. The electrons are removed from the graphene layer via the cyano groups of the molecule. Since the molecules remain stable under ambient conditions, at elevated temperatures and can be applied via wet chemistry this doping method is attractive as its incorporation into existing technological processes appears feasible. In bilayer graphene, the hole doping allows the Fermi level to shift into the energy band-gap and the additional dipole developing at the interface with the F4-TCNQ overlayer causes the band-gap magnitude to increase to more than double of its original value. Thus, the electronic structure of the graphene bilayer can be precisely tuned by varying the molecular coverage.

*c.coletti@fkf.mpg.de

†u.starke@fkf.mpg.de; http://www.fkf.mpg.de/ga

[1] K. S. Novoselov, A. K. Geim, S. V. Morozov, D. Jiang, Y. Zhang, S. V. Dubonos, I. V. Grigorieva, and A. A. Firsov, Science **306**, 666 (2004).

[2] K. S. Novoselov, A. K. Geim, S. V. Morosov, D. Jiang, M. I. Katsnelson, I. V. Grigorieva, S. V. Dubonos, and A. A. Firsov, Nature (London) **438**, 197 (2005).

[3] Y. Zhang, Y.-W. Tan, H. L. Stormer, and P. Kim, Nature (London) **438**, 201 (2005).

[4] C. Berger, Z. Song, X. Li, X. Wu, N. Brown, C. Naud, D. Mayou, T. Li, J. Hass, A. N. Marchenkov, E. H. Conrad, P. N. First, and W. A. de Heer, Science **312**, 1191 (2006).

[5] C. Riedl, U. Starke, J. Bernhardt, M. Franke, and K. Heinz, Phys. Rev. B **76**, 245406 (2007).

[6] K. V. Emtsev, A. Bostwick, K. Horn, J. Jobst, G. L. Kellogg, L. Ley, J. L. McChesney, T. Ohta, S. A. Reshanov, E. Rotenberg, A. K. Schmid, D. Waldmann, H. B. Weber, and T. Seyller, Nature Mater. **8**, 203 (2009).

[7] T. Ohta, A. Bostwick, T. Seyller, K. Horn, and E. Rotenberg, Science **313**, 951 (2006).

[8] T. Ohta, A. Bostwick, J. L. McChesney, T. Seyller, K. Horn, and E. Rotenberg, Phys. Rev. Lett. **98**, 206802 (2007).

[9] S. Y. Zhou, G.-H. Gweon, A. V. Fedorov, P. N. First, W. A. de Heer, D.-H. Lee, F. Guinea, A. H. Castro Neto, and A. Lanzara, Nature Mater. **6**, 770 (2007).

[10] C. Riedl, A. A. Zakharov, and U. Starke, Appl. Phys. Lett. **93**, 033106 (2008).

[11] A. Bostwick, T. Ohta, T. Seyller, K. Horn, and E. Rotenberg, Nat. Phys. **3**, 36 (2007).

[12] C. Riedl, C. Coletti, T. Iwasaki, A. A. Zakharov, and U. Starke, Phys. Rev. Lett. **103**, 246804 (2009).

[13] T. O. Wehling, K. S. Novoselov, S. V. Morozov, E. E. Vdovin, M. I. Katsnelson, A. K. Geim, and A. I. Lichtenstein, Nano Lett. **8**, 173 (2008).

[14] T. Lohmann, K. von Klitzing, and J. H. Smet, Nano Lett. **9**, 1973 (2009).

[15] J. Kong, N. R. Franklin, C. Zhou, M. G. Chapline, S. Peng, K. Cho, and H. Dai, Science **287**, 622 (2000).

[16] P. G. Collins, K. Bradley, M. Ishigami, and A. Zettl, Science **287**, 1801 (2000).

[17] S. Y. Zhou, D. A. Siegel, A. V. Fedorov, and A. Lanzara, Phys. Rev. Lett. **101**, 086402 (2008).

[18] F. Schedin, A. K. Geim, S. V. Morozov, E. W. Hill, P. Balke, M. I. Katsnelson, and K. Novoselov, Nature Mater. **6**, 652 (2007).

[19] V. Derycke, R. Martel, J. Appenzeller, and Ph. Avouris, Appl.

Phys. Lett. **80**, 2773 (2002).

[20] W. Chen, D. Qi, X. Gao, and A. T. S. Wee, Prog. Surf. Sci. **84**, 279 (2009).

[21] Q. Su, S. Pang, V. Alijani, C. Li, X. Feng, and K. Müllen, Adv. Mater. **21**, 3191 (2009).

[22] E. Bekyarova, M. E. Itkis, P. Ramesh, C. Berger, M. Sprinkle, W. A. de Heer, and R. C. Haddon, J. Am. Chem. Soc. **131**, 1336 (2009).

[23] Y. H. Lu, W. Chen, Y. P. Feng, and P. M. He, J. Phys. Chem. B **113**, 2 (2009).

[24] J. Choi, H. Lee, K.-J. Kim, B. Kim, and S. Kim, J. Phys. Chem. Lett. **1**, 505 (2010).

[25] W. Chen, S. Chen, D. C. Qui, X. Y. Gao, and A. T. S. Wee, J. Am. Chem. Soc. **129**, 10418 (2007).

[26] X. Zhou, M. Pfeiffer, J. Blochwitz, A. Werner, A. Nollau, T. Fritz, and K. Leo, Appl. Phys. Lett. **78**, 410 (2001).

[27] J. Blochwitz, M. Pfeiffer, T. Fritz, and K. Leo, Appl. Phys. Lett. **73**, 729 (1998).

[28] Z. Q. Gao, B. X. Mi, G. Z. Xu, Y. Q. Wan, M. L. Gong, K. W. Cheah, and C. H. Chen, Chem. Commun. (Cambridge) (2008), 117.

[29] S. Kazaoui, Y. Guo, W. Zhu, Y. Kim, and N. Minami, Synth. Met. **135-136**, 753 (2003).

[30] T. Takenobu, T. Kanbara, N. Akima, T. Takahashi, M. Shiraishi, K. Tsukagoshi, H. Kataura, Y. Aoyagi, and Y. Iwasa, Adv. Mater. **17**, 2430 (2005).

[31] Y. Nosho, Y. Ohno, S. Kishimoto, and T. Mizutani, Nanotechnology **18**, 415202 (2007).

[32] G. Gao and A. Kahn, Appl. Phys. Lett. **79**, 4040 (2001).

[33] W. Gao and A. Kahn, Org. Electron. **3**, 53 (2002).

[34] H. Pinto, R. Jones, J. P. Goss, and P. R. Briddon, J. Phys.: Condens. Matter **21**, 402001 (2009).

[35] S. Soubatch, S. E. Saddow, S. P. Rao, W. Y. Lee, M. Konuma,

and U. Starke, Mater. Sci. Forum **483-485**, 761 (2005).

[36] C. L. Frewin, C. Coletti, C. Riedl, U. Starke, and S. E. Saddow, Mater. Sci. Forum **615-617**, 589 (2009).

[37] T.-C. Tseng, C. Lin, X. Q. Shi, S. L. Tait, X. Liu, U. Starke, N. Lin, R. Q. Zhang, C. Minot, M. A. Van Hove, J. I. Cerda, and K. Kern, Phys. Rev. B **80**, 155458 (2009).

[38] S. K. Wells, J. Giergel, T. A. Land, J. M. Lindquist, and J. C. Hemminger, Surf. Sci. **257**, 129 (1991).

[39] J. M. Lindquist and J. C. Hemminger, J. Phys. Chem. **92**, 1394 (1988).

[40] L. Romaner, G. Heimel, J.-L. Bredas, A. Gerlach, F. Schreiber, R. L. Johnson, J. Zegenhagen, S. Duhm, N. Koch, and E. Zojer, Phys. Rev. Lett. **99**, 256801 (2007).

[41] D. Qi, W. Chen, X. Gao, L. Wang, S. Chen, K. P. Loh, and A. T. S. Wee, J. Am. Chem. Soc. **129**, 8084 (2007).

[42] N. Koch, A. Rajagopal, J. Ghijsen, R. L. Johnson, G. Leising, and J.-J. Pireaux, J. Phys. Chem. B **104**, 1434 (2000).

[43] N. Koch, S. Duhm, J. P. Rabe, A. Vollmer, and R. L. Johnson, Phys. Rev. Lett. **95**, 237601 (2005).

[44] D. S. Lee, C. Riedl, B. Krauss, K. v. Klitzing, U. Starke, and J. H. Smet, Nano Lett. **8**, 4320 (2008).

[45] J. Röhrl, M. Hundhausen, K. V. Emtsev, T. Seyller, R. Graupner, and L. Ley, Appl. Phys. Lett. **92**, 201918 (2008).

[46] J. Yan, Y. B. Zhang, P. Kim, and A. Pinczuk, Phys. Rev. Lett. **98**, 166802 (2007).

[47] A. Das, S. Pisana, B. Chakraborty, S. Piscanec, S. K. Saha, U. V. Waghmare, K. S. Novoselov, H. R. Krishnamurthy, A. K. Geim, A. C. Ferrari, and A. K. Sood, Nat. Nanotechnol. **3**, 210 (2008).

[48] E. McCann and V. I. Fal'ko, Phys. Rev. Lett. **96**, 086805 (2006).

[49] The band velocity v_B equals 1.07×10^6 m/s. The dimer coupling γ_1 varies from 0.40 eV for the clean bilayer to 0.52 eV for a bilayer with molecular film coverage of 1.5 nm. The next-nearest-neighbor coupling γ_3 remains fixed at 0.12 eV.